# Journal of Materials Chemistry A

Accepted Manuscript






ROYAL SOCIETY OF CHEMISTRY

www.rsc.org/materialsA

# Thermal, electrical and structural studies on ionic liquid confined in ordered mesoporous MCM-41

Alok Kumar Tripathi, Yogendra Lal Verma and Rajendra Kumar Singh*
Department of Physics, Banaras Hindu University, Varanasi-221005, India

## Abstract

In the present study, immobilization of different amount of ionic liquid (IL) 1-ethyl-3-methyl imidazolium tetrafluoroborate [EMIM][$BF_4$] into the pores of ordered mesoporous MCM-41 (Mobil Composition of Matter No. 41) has been accomplished successfully. Differential scanning calorimetry (DSC) and dielectric spectroscopy results indicate the presence of surface adsorbed IL besides, IL confined in pores. The IL adsorbed on the surface of MCM-41 has been removed after washing. DSC and dielectric spectroscopy results and scanning electron microscopy (SEM) confirm the removal of the surface adsorbed IL. Glass transition temperature ($T_g$) and thermal stability have been found to change as compared to the bulk IL in confinement. FTIR study shows that the vibrational bands related to the ring of the IL cation shift upon confinement due to the interaction between oxygen of silica pore wall surface and C-H of the cation ring. Anion $[BF_4]^-$ also interacts with the pore wall as confirmed experimentally and theoretically. Fluorescence spectra of IL show the blue shift upon incorporation into the ordered mesoporous MCM-41.

---

Corresponding Author e-mail: *rksingh_17@rediffmail.com and *rajendrasingh.bhu@gmail.com Tel. +91 542 6701541; Fax +91 542 2368390

## 1. Introduction

Ionic liquids (ILs) are the subject of a large number of the research studies due to their unique chemical and physical properties[1] and characteristics different from conventional molecular liquids. The ILs are composed of organic cations and organic/inorganic anions.[2] Due to diverse functionality, they exhibit dispersive, π–π, hydrogen bonding, dipolar and ionic/charge-charge interactions.[3] ILs have exotic properties like low vapor pressure, high thermal and chemical stability, high ionic conductivity, wide liquidus range, wide electrochemical window etc.[1] Due to these interesting properties, ILs have been used in catalysis,[4] electrochemical devices (e.g. batteries, supercapacitors etc.),[5-7] separation technologies,[8] green chemistry[9] and other applications. These properties make it a better salt but liquidus nature and rather specific physical properties like high viscosity and low diffusion coefficients[1] hinder its use in many applications.

To overcome some limitations due to the liquidus nature, it has been proposed that ILs can be applied onto porous support surfaces. ILs confined in nanoporous matrices have recently resulted an advanced class of materials called Ionogel (IG).[10] The ionogels are suitable candidates for applications in many devices such as supercapacitor, rechargeable battery, fuel cell, electrochemical sensor, biosensor, catalysis, optical solvent, biocatalysis etc.[10-16] The properties of ILs viz. phase transition temperature, thermal stability, optical properties, etc. have been found to change upon confinement.[17-20] Porous gel matrices prepared by different methods may result in changes in the average pore size, pore size distribution, porosity, pore volume, surface area etc. depending upon the composition of the starting material, mode of synthesis, temperature etc.

In our recent studies, ILs have been confined using hydrolytic and non-hydrolytic sol-gel routes[20-22] in which properties of ILs and porous structure of matrices were investigated. These processes had some limitations like longer synthesis and aging times of ionogels, rare monolith formation, large shrinkage during aging, cost of metallic precursors etc. One important demerit was that these processes did not yield ordered and homogeneous pores i.e. ILs were not immobilized in continuous porous channel. To overcome these shortcomings a new method has been adopted for immobilizing IL into the ordered mesoporous materials.

Ordered porous materials are a special class of materials, which have aroused great interest because of their attractive textural features (larger pore diameters and large specific surface areas) and aspects for related applications. Different types of ordered porous solids have been synthesized, such as zeolites (crystalline 3D framework with microporous structures),[23] M41S family of silica-based mesoporous materials,[24,25] SBA (Santa Barbara Amorphous)-type ordered mesoporous silica,[24,26] CPG (controlled pore glasses)[27] etc. In addition to these ordered porous solids some new mesoporous materials are also synthesized e.g. mesoporous organosilicas (PMOs),[28] metal-organic frameworks (MOFs),[29] and covalent organic frameworks (COFs).[30] Both, SBA-15 and MCM-48 have similar porous nature but in SBA-15 pores are unidirectional in ordered hexagonal topology while MCM-48 possesses three-dimensional (3D) cubic structures of the pores. CPG is also a porous matrix which consists an amorphous network of pores of uniform size with a surface that consists of siloxane and silanol groups which provide attachment sites. However, MCM 41 is typical mesoporous templated silica which is most frequently used. MCM 41 exhibits exciting structural features like large specific surface area (upto 1000 $m^2/g$) and ordered cylindrical mesopores with a narrow size distribution and its inner structure consists of unidirectional channel-like pores that form a hexagonal pattern. These ordered mesoporous

materials have been used as support in various fields viz. drugs,[31] liquid crystals,[32] enzymes,[33] catalysis,[34] etc. Recently, ILs have been incorporated in MCM-41 and other ordered mesoporous materials via different process[35] such as grafting,[36] ion exchange,[37] slurry impregnation[38] method etc. After immobilization of IL into these ordered matrices, the materials are defined as SILP (supported ionic liquid phase) materials that feature a solid porous support containing a certain amount of physisorbed and/or covalently anchored ionic liquid. Vangeli et al.[36] immobilized the IL ([SPMIM][$PF_6$]) in MCM-41 and SBA-15 by using grafting method and studied the thermal and physical properties of IL. Stefanopoulos et al.[24] also reported the information about orientation of IL molecules during the filling of IL [BMIM][$PF_6$], in the pores of MCM-41 and SBA-15. However, still there is limited literature available on studies on physicochemical properties of ILs immobilized on uniform mesoporous materials.

In the present study, we are interested in finding the properties of IL incorporated into available pore space of MCM-41. One of the important issues for the confinement of IL into ordered porous matrices is the degree of pore filling, because space between external pore surfaces of cylindrical walls offers additional space where IL can be absorbed besides being confined into the pores. Recently, by using SANS (Small-angle neutron scattering) and $N_2$-adsorption method, Stefanopoulos et al.[24] reported the pore filling of SBA-15 and MCM-41 by the IL [BMIM][$PF_6$]. Since during pore filling, a fraction of IL may get entrapped into the space between external surfaces of cylindrical walls (this IL referred as surface absorbed IL) so, in order to study the properties of IL confined within the pores, surface adsorbed IL needs to be removed because the surface adsorbed IL may have properties different than the confined IL. However, only sporadic studies mention about the surface adsorbed IL besides IL entrapped within the pores.[39,40] So, in the present study, we have used a novel route to confine IL within the pores. The IL entrapped on

external surface of cylindrical walls has been removed. Glass transition results showed the signature of surface adsorbed IL, which was washed to obtain MCM-41 containing confined IL only. Also, in the present study we attempt to show that the dielectric relaxation measurements can be used as a tool to verify the change in the dynamical behavior of ionic liquid confined into pores. It also confirms that the surface bound ionic liquid was successfully removed from the outer surface of the MCM-41 matrix.

## 2. Experimental section

### 2.1. Materials.

The IL [EMIM][$BF_4$] (of stated purity > 98.9% with halide content less than 10 mg/Kg) and MCM-41 were purchased from Sigma-Aldrich. To protect the IL from humidity, it was handled under a dry nitrogen atmosphere. Solvent methanol (99.8%, Aldrich) was used as purchased. Prior to use, IL was vacuum (~$10^{-3}$ torr) dried at 100 °C for 24 h before storing in a glove box. To analyze the water content in IL, Karl Fischer Coulometric Titrator (Mettler Toledo C20) was used. The water content was less than 50 ppm**.**

### 2.2. Synthesis Process.

The pore filling of the samples with IL was achieved by vacuum assisted physical imbibition of [EMIM][$BF_4$] from its methanol solution. MCM-41 powder was placed on the bottom of a vial (a bottom-flat, two-way glass valve and the sidewall of the vial closed to its beveled neck) along with stirring magnet (see Fig. 1). For this two way valve, one port was used as vacuum working port and other was tightly sealed. After drying MCM-41 powder for 24 h, a binary mixture of IL and excess methanol was injected on the powder. The powder suspension was ultrasonicated by

keeping the vial in water for 30 min. In this process, more and more IL enters into the pores without breaking vacuum. After that the suspension was stirred for several hours. At last some amount of sample was taken away (labeled as M-3, M-4 and M-5 containing 30, 40 and 50 wt.% IL respectively) and remaining was washed by the methanol several times to remove surface IL (samples labeled as MW-3, MW-4 and MW-5 which indicate 30, 40 and 50 wt.% IL samples with surface adsorbed IL washed away). The amount of IL obtained after washing surface adsorbed IL from M-3, M-4, and M-5 is 7, 9 and 16 wt.% respectively, which was determined by weighing the IL obtained after evaporating the solvent (methanol). So, the actual amount of IL present in the samples; MW-3, MW-4 and MW-5 is 23, 31 and 34 wt.% respectively. After synthesis of ionogels (IL immobilized MCM-41), its physical appearance was in the powder form as shown in Fig. 2.

**2.3. Characterization.**

A Mettler Toledo DSC-1 (differential scanning calorimeter) was used to determine phase transition temperature. The requisite amount of sample was placed in 40 µl hermetically sealed aluminium pan with pinhole at the top of the pan. Each sample was vacuum dried at 80 $^{o}$C for 5 h before the experiment. The measurements were carried out by first heating the samples at 100 $^{o}$C for 20 min to remove the absorbed water and then cooling the samples to -110 $^{o}$C followed by an isotherm for half an hour at -110 °C and then the DSC thermograms were recorded from -110 °C to 100 °C with fixed scan rate of 10 °C min$^{-1}$.

Dielectric measurement was carried out using Novocontrol (Alpha A) Impedance Analyzer, in the frequency range of 1 Hz to 10 MHz. The IL confined MCM-41 samples were sandwiched

between two gold plated electrodes and subjected to the dielectric measurement. Temperature-dependent dielectric measurement was carried out from 40 to 100 $^{o}$C.

To obtain the pore parameters (BET surface area, pore volume, average pore diameter), $N_2$-sorption measurement was carried out at 77 K using Gemini VII 2390t model of Micromeritics Instrument Corporation. Before the measurement, all the samples were degassed under flow of dry $N_2$ for 24 h at 60 $^{o}$C.

Surface morphological investigations of the samples were analyzed by using scanning electron microscope (SEM) Magellan 400.

TEM images of samples were obtained on a Tecnai $G^2$F30.

Thermal stability of IL confined in MCM-41 was obtained by thermogravimetric analysis (TGA). TGA was carried out with Mettler Toledo TGA/DSC 1 analyser. All the samples were run in alumina ($Al_2O_3$) pan at a heating rate of 10 $^{o}$C min$^{-1}$ under $N_2$ atmosphere. Before the measurement, all the samples were dried at 100 $^{o}$C for 12 h.

The FTIR spectra were recorded using Perkin Elmer spectrum 65 FTIR spectrometer. The pristine MCM-41 and IL confined samples were taken in very small amount and dispersed in KBr and then pelletised for recording the FTIR spectra. For recording the spectra of bulk IL, a very small amount of IL was used to wet the KBr pellet.

The Fluorescence spectra were recorded at room temperature with a Perkin Elmer LS 45 Fluorescence Spectrometer with a pulsed xenon lamp as excitation source and a photomultiplier tube as detector.

## 3. Results and Discussion

### 3.1. DSC

In order to investigate the effect of confinement on the IL, DSC is very useful technique because the properties of a liquid confined into porous materials are different from those of the liquid in the bulk.[41] Since, physicochemical properties of ionic liquids change in the presence of impurities like water, organic solvents and halide ions.[42,43,44] Therefore, prior to confining IL into mesoporous MCM-41 support, IL as well as IL containing MCM-41 mesoporous materials were dried at 100 ˚C under vacuum ($10^{-3}$ torr). Fig. 3a and 3b show the DSC thermograms of bulk IL ([EMIM][$BF_4$]) and confined IL into nano pores of MCM-41 (M-5 and MW-5), respectively. Fig. 3a shows that there are two crystallization and two melting peaks present in the bulk IL as reported in our earlier studies for in-situ entrapment of IL using non-hydrolytic sol-gel process.[21] However, upon incorporation of the IL into MCM-41 (M-5, containing higher amount of IL), two glass transition temperatures have been found (shown in Fig. 3b curve (i)) while, no crystallization and melting peaks are found. The absence of these two peaks may be due to the dispersal of IL into the uniform porous material MCM-41. Here, the two glass transition temperatures are attributed to the surface adsorbed ($T_{g_1}$ ~ -92 °C) and confined IL into the nanopores of MCM-41 ($T_{g_2}$ ~ -80 °C). From the Fig. 3b, it can be seen that the glass transition temperature $T_{g_1}$ is nearly equal to the glass transition temperature of bulk IL ($T_g$ ~ -94 °C) shown in Fig. 3a; i.e. surface adsorbed IL behaves like bulk IL. Furthermore, the glass transition temperature of confined IL has been found to change as compared to the bulk IL ($\Delta T_g$ ~14 °C).

This change in the glass transition temperature of confined IL may be due to the interaction of IL molecules with MCM-41 pore wall surface.[45,46] Unlike our earlier study for in situ confined IL ([EMIM][$BF_4$]) into the $SiO_2$ matrix, in which we found that the crystallization, $T_{c,}$ and melting, $T_{m,}$ temperatures shift as compared to the bulk IL but in the present study upon confinement of IL in ordered mesoporous material, only the glass transition temperature ($T_g$) is found. Further, to confirm that $T_{g_1}$ corresponds to the surface adsorbed IL, we have washed the surface adsorbed IL of sample M-5 (resulting sample termed as MW-5). DSC thermogram of surface washed sample containing higher amount of IL (MW-5) is given in Fig. 3b (curve (ii)), which shows that MW-5 has only a single glass transition temperature at ~ -80 °C, corresponding to the IL confined in mesopores of MCM-41, which shows about ~14 °C change compared to the bulk IL due to the interaction of IL molecules with the pore wall surface.

Overall, the DSC study reveals the signature of surface adsorbed IL as well as confined IL in nanopores of MCM-41 for the as prepared sample (before washing the samples) and also confirms the removal of surface adsorbed IL. This observation has been confirmed by impedance spectroscopy measurement (as discussed in next section), where, we have observed two peaks in the electric modulus vs log f plots for unwashed IL sample and single modulus peak for washed sample.

### 3.2. Impedance Spectroscopy

Impedance spectroscopy is well suited technique to investigate the dynamics of ionic liquid into confined system. From DSC results, two $T_g$ values were found for IL which reveals that the ionic liquid gets dispersed in (i) pores of matrix and (ii) space between the external surface of the pore

wall, so the associated relaxation processes are expected to be different because of their different surrounding space.

Dielectric relaxation can be obtained in terms of complex relative permittivity, ε*, or loss tangent, tan δ, plots with respect to log of frequency (f). But at low frequencies, the charges get accumulated at the interfacial region that leads to a net polarization and gives electrode polarization phenomenon.[47] The electric modulus plots suppress the electrode polarization effect and can be used to distinguish effects having very close modulus values. The electric modulus has been used to interpret electrical relaxation data in a wide variety of materials. This formalism provides wider insights on charge transport processes such as mechanism of conductivity relaxation and ion dynamics as a function of frequency and temperature. In the modulus formalism,[48] an electrical modulus M* is defined as the reciprocal of the complex relative permittivity ε*

$$M^* = 1/\varepsilon^* = M' + iM'' \quad (1)$$

Where M' and M'' are its real and imaginary parts respectively. Fig. 3a and 3b show the imaginary part (M'') of electrical modulus as a function of log of frequency (log f) for bulk ionic liquid and M-3 (without wash sample containing 30 wt.% IL) at 40 $^{o}$C and inset of Fig. 4b shows the M″ vs log f plot for the surface adsorbed IL washed sample MW-3. From Fig. 4a, the low value of M″ in the low frequency region indicates a negligible contribution of electrode polarization to the electric modulus. A relaxation in bulk ionic liquid appears to be at higher frequencies (far more than 10 MHz) and the corresponding peak relaxation frequency, $f_r$, shifts towards the higher frequency region with temperature. From Fig. 4b it is clear that there are two relaxation peaks in the Modulus spectra for sample M-3 which suggests that the relaxation

behavior is associated with two different processes. One peak is found in the region between $10^3$ to $10^4$ Hz and other is near the frequency region 10 MHz. The relaxation at lower frequency region is found due to the surface adsorbed IL because of its slower dynamics due to the adherence on surface. As temperature increases, the lower relaxation frequency region shifts towards higher frequency side which tells that the adherence force between surface and IL becomes weaker.

For sample MW-3 (in which surface adsorbed IL has been removed), inset of Fig. 4b shows that the surface adsorbed IL is successfully removed and only one relaxation peak at higher frequency region is found, for which relaxation frequency is less than the relaxation frequency corresponding to the bulk IL. Thus, we can say that after removal of surface adsorbed IL, samples contain IL into the pores only.

### 3.3. BET ANALYSIS

$N_2$-sorption is an essential characterization technique to investigate the pore parameters of porous materials. Therefore, in the present study, $N_2$ adsorption-desorption measurement has been carried out to observe pore parameters. The specific surface area has been determined by the BET method.[49] Fig. 5a and 5b illustrate the $N_2$-sorption isotherms of pristine MCM-41 and MW-3, MW-4 and MW-5. The pore parameters of pristine and IL treated MCM-41 samples are given in Table 1. The average pore size of pores in pristine MCM-41 is ~ 3.4 nm. From the Fig. 5a, it can be seen that the isotherm of pristine MCM-41 exhibits the type IV characteristics with type H1 hysteresis loop; according to IUPAC classification.[50] At low relative pressures ($0.3<P/P_0<0.5$); a steep increase is observed which is ascribed to the uniform cylindrical pore structure.[24] However, at high relative pressure, hysteresis loop is due to capillary condensation

and evaporation on open cylindrical pores at both ends. The upturns of the isotherm in pristine MCM-41 at relative pressure $P/P_0$ close to 1 is attributed to the formation of large mesoporous pores due to the MCM-41 interparticles.[51] However, surface adsorbed IL washed samples (MW-3, MW-4 and MW-5) also exhibit type IV isotherm characteristics.

From the Table 1, it can be seen that as the amount of IL incorporation is increased, the pore volume, porosity and BET constant C decreased. The decrease in the value of BET constant C with increasing IL loading reveals that more amount of IL in the pores is physisorbed. The BET constant C is interpreted as a parameter describing the interaction between $N_2$ molecules with surface of pores. The % porosity of samples has been calculated using the BJH equation;

$$\% \text{ porosity, } \phi = \frac{\text{BJH pore volume}}{\text{BJH pore volume} + \frac{1}{\rho}} \qquad (2)$$

Where ρ is density of silica (2.2 gm/cm$^3$).[52]

However, for the samples (M-3, M-4 and M-5), we have not observed the isotherm during the $N_2$-sorption measurement. Because $N_2$ is not dissolved in a particular, IL, phase. In this case, we can say that either total pores are filled with IL or pores are blocked due to the surface adsorbed IL. But, the amount of IL taken for the incorporation in these samples (M-3, M-4 and M-5) is small as compared to the specific pore volume of MCM-41. So, the absence of isotherm during $N_2$-sorption experiment may be due to the blockage of pore mouths and partially filled pores. The absence of isotherms due to the blocking of hexagonal pores of MCM-41 is schematically shown in Fig. 6. The Fig. 6a shows that IL seeps inside the pores through the pore walls while Fig. 6b shows how the pores may be blocked by building layer between the pore wall either deep

inside the pores or at the mouth of the pores. The Fig. 6c shows the schematic representation of filling of IL at pore mouth and how the blockage at pore mouth prevents further filling of IL inside the pores. This schematic diagram shows that a very thin layer of IL is present at external pore wall surface and on pore mouth which reflects as surface adsorbed IL. However, IL adsorbed on the pore mouth restricted the filling of IL into pores.

### 3.4. SEM

The typical SEM images of MCM-41, M-5 and MW-5 are given in Fig. 7a, 7b and 7c respectively. The morphology of the sample (M-5/MW-5) was similar to but smoother than the MCM-41. However, a thin film appeared on the surface of M-5 (before washing the surface adsorbed IL) as shown in Fig. 7b which confirms that ionic liquid is present on the surface, while SEM micrograph of sample MW-5 reveals that the surface adsorbed IL has been removed completely during washing.

### 3.5. TEM

The typical TEM images of MCM-41 and MW-5 are shown in Fig. 8. The TEM image of MCM-41 (Fig. 8a) reveals the two characteristic features present abundantly in the pristine MCM-41. These features include (i) parallel lines with variable spacing (in square) and (ii) a honeycomb structure (in circle) (Fig. 8a). We found that most of the particles lie along the length of the honeycomb tubes on the specimen plane. Since many particles in the powder sample appear laying flat on the specimen plane due to the stable configuration of the particles. The ordered honeycomb faces are not observed as frequently as the parallel lines. In Fig. 8a, parallel lines have wide spacing and narrow spacing (in square) due to the projections along two symmetry

orientations.[53] In honeycomb view, the lattice constant, a, is found to be 4.12 nm, which is the distance from pore centre to the adjacent pore centre. From BET results, average pore diameter is 3.4 nm. Therefore, the width of the MCM-41 wall is ~0.63 nm. Fig. 8b shows the TEM image of sample MW-5 (containing higher amount of IL after washing of surface adsorbed IL) which shows that the mesoporous structure of MCM-41 is still retained after the incorporation of IL. It can also be seen that the IL is not present on the surface.

### 3.6. TGA

Fig. 9a and 9b show the TGA thermograms of pristine MCM-41; bulk IL and IL confined MCM-41 samples after the washing of the surface adsorbed IL (MW-3, MW-4 and MW-5). Thermogram of pristine MCM-41(Fig. 9a) shows very small weight loss ~2.8 wt.% in the temperature range 40-600 $^{o}$C. This small amount of %weight loss occurs due to physically (~1.6 wt.%) and chemically (~1.2 wt.%) adsorbed water in the pristine MCM-41 due to unintentional unhydrolyzed hydroxyl groups (OH-groups) present.[54] Further, TGA thermograms (Fig. 9b) of samples (MW-3, MW-4 and MW-5) reveal that thermal stability is decreased upon confinement of IL in MCM-41. The cause of decrease in thermal stability is the interaction of IL molecules to the pore wall surface. As, we have observed theoretically and experimentally (given in section 3.7) that C-H of the imidazolium ring is interacting with oxygen of pore wall surface. Thus due to these interactions IL molecules may hinge in the nanopores of MCM-41 and thermal stability of the confined IL is decreased.[18] The onset decomposition temperature and %weight loss of bulk IL and confined IL are given in Table 2, which reveals that as the amount of IL is increasing, the onset decomposition temperature of confined IL goes near the onset temperature of bulk IL. From the TGA thermograms of bulk IL and confined IL (as shown in Fig. 9b), it can

also be seen that after complete decomposition of bulk IL and samples; MW-3, MW-4 and MW-5, the %weight loss of IL is approximately to 98, 20, 28 and 33 wt.% respectively. Thus we can say that the amount of entrapped IL in samples MW-3, MW-4 and MW-5 is nearly equal to the calculated amount of the entrapped IL (23, 31 and 34 wt.%, respectively) as mentioned in section 2.2.

Since, the density of hydroxyl groups in the MCM-41 gives the important information about the interactions between OH groups and confined IL. Therefore, in the present study, we have also calculated the OH density by using TGA analysis. The number of hydroxyl groups per unit $nm^2$, ($\alpha_{OH}$), on the surface of the MCM-41 can be calculated using the following equation,[55]

$$\alpha_{OH} = \delta_{OH} \times N_A \times 10^{-21}/S \quad (3)$$

Where $\delta_{OH}$ (mmol OH groups/g of MCM-41) is the concentration of OH groups on the surface of MCM-41 per unit mass of the sample, S ($m^2/g$) is the specific surface area of the sample as obtained by the BET method, $N_A$ is the Avogadro number. The hydroxyl group content of the MCM-41, $\delta_{OH}$ (mmol/g), can be calculated as:

$$\delta_{OH} = \frac{2[WL(T_0) - WL(T_{final})] \times 10^3}{100 \times M_{H_2O}} \quad (4)$$

Where $M_{H_2O}$ is the molar mass of water and $[WL(T_0) - WL(T_{final})]$ is the weight loss (wt.%) in the temperature region $T_0 - T_{final}$ (where $T_0$ is the temperature of onset and $T_{final}$ is the temperature of endset of the decomposition) obtained from the TGA thermogram as shown in Fig. 9a. From the calculation we have obtained that the concentration of OH groups is ~0.98 per $nm^{-2}$ in pristine MCM-41, which is very small (the density of the hydroxyl groups cannot be higher than 4.9 OH

$nm^{-2}$).[56,57] Thus in our case, smaller amount of OH groups present in the MCM-41 brings out that the prominent interaction of IL will occur with O-Si-O only.

### 3.7. FTIR

To study the interaction of ionic liquid molecules with the silica (MCM-41) pore wall surface, FTIR studies were carried out. The FTIR spectra of bulk IL, MW-3, MW-4 and MW-5 (in the spectral range 3210-2800 $cm^{-1}$) are shown in Fig. 10a. The vibrational bands of the bulk and confined IL samples (MW-3, MW-4 and MW-5) with their assignments are given in Table 3. Fig. 10a shows the vibrational bands related to the C-H vibrations of aromatic ring and alkyl chain of the imidazolium cation. From the Table 3 it can be seen that the vibrational bands at 3167 $cm^{-1}$ and 3123 $cm^{-1}$ are ascribed to H-C(4)-C(5)-H and C(2)-H stretching of the imidazolium ring respectively as shown in Fig. 11 (optimized structure of IL).[58,59] However, upon confinement of IL in MCM-41 obtained FTIR spectrum is different. From the Figure 10a it can be seen that the intensity of vibrational bands related to H-C(4)-C(5)-H and C(2)-H of IL is very low and it decreases as the amount of IL in MCM-41 decreases. These vibrational bands are found to shift as compared to the bands of the bulk IL [Table 3]. Deng et al.[60] have also found an abnormal FTIR spectra for different confined IL in silica matrix due to the change in the amount of IL and pore size of silica matrix. From the Fig. 10a, it can be seen that upon confinement of IL in nanopores of MCM-41, the change observed in vibrational bands of C(2)-H and H-C(4)-C(5)-H is about 4-6 $cm^{-1}$ and 3-4 $cm^{-1}$ respectively. The larger shift in vibrational bands of C(2)-H may be due to the strong interaction between oxygen of the silica pore wall surface and more acidic C(2)-H site of the imidazolium cation as compared to the H-C(4)-C(5)-H.[61,62,63,64,65] Peaks assigned to the C-H stretching of the alkyl chain of bulk IL are observed at 2993 $cm^{-1}$, 2950 $cm^{-1}$

and 2890 $cm^{-1}$.[58,59] While, upon confinement of IL the intensity of these peaks decreases as content of IL in MCM-41 decreases. Therefore, the vibrational bands related to the C-H stretching of the alkyl chain are not clearly visible except the bands at 2995 $cm^{-1}$ and 2996 $cm^{-1}$ for the sample MW-5 and MW-4 respectively. It can be seen that vibrational bands of bulk IL related to the C-H of the alkyl chain is also shifted ~ 2-3 $cm^{-1}$ upon confinement which is smaller than the shift for C-H vibration of the ring.

Fig. 10b and 10c, shows the FTIR spectra (in spectral range 1300-400 $cm^{-1}$) of bulk IL, MW-3, MW-4, MW-5 and MCM-41 and the vibrational bands with assignments are listed in Table 3. In this spectral range the following changes have been found:

1. It has been observed that the vibrational bands related to $[BF_4]^-$ anion of the bulk IL (Fig. 10b) at 757 $cm^{-1}$, 1024 $cm^{-1}$, 1060 $cm^{-1}$, 1116 $cm^{-1}$ and 1173 $cm^{-1}$ are found to shift upon confinement for all the samples as given in Table 3.[25,58,66,67] From the Table 3 it can be seen that the vibrational band at 1024 $cm^{-1}$ related to the asymmetric stretching of the bulk IL shows a large shift ~ 23 $cm^{-1}$.

2. Vibrational bands related to MCM-41 (given in Fig 10b) at 464 $cm^{-1}$ (bending of Si-O-Si), 800 $cm^{-1}$ (stretching of Si-O), 969 $cm^{-1}$ (symmetric stretching of Si-OH) and 1086 $cm^{-1}$ (internal asymmetric of Si-O) are also much affected for the samples MW-3, MW-4 and MW-5.[26,68]

Recently, it has been reported by using theoretical calculation that C-H of the imidazolium ring interacts with the oxygen of the silica pore wall surface.[17,55] In the present investigation, we have also adopted a theoretical approach (DFT calculations) to confirm these interactions. For this, we

have optimized the geometries of IL and IL in the presence of $SiO_2$ using Gaussian 09 package[64] by DFT method with the basis set B3LYP, 3-21G (Becke's three-parameter exchange functional[65] in combination with the Lee, Yang, and Parr correlation functional[66]). Internal co-ordinates were generated using the Gauss View 05 program[67] which was used as an input to the main Gaussian programme. To optimize the structures of IL in the presence of $SiO_2$ and to see the interaction of IL with $SiO_2$, the programme was run with different trial inputs by placing the $SiO_2$ near IL molecules having different orientations. Trial inputs are as follows and their outputs obtained from the calculation are shown in Fig. 12.

1. Trial 1: input was such that C-H of the ring was forced to interact with O of $SiO_2$.

2. Trial 2: input was such that anion $[BF_4]^-$ of IL interacts with $SiO_2$.

3. Trial 3: $SiO_2$ was allowed to interact with both cation as well as anion from both sides. One $SiO_2$ was near C-H of the cation ring and another was near to the anion.

From the output of first trial run, it can be seen that oxygen of $SiO_2$ interacts with the H-C(4) and C(5)-H of imidazolium ring. In the output of second trial run, oxygen and silicon (Si) of silica ($SiO_2$) interact with H-C(2) of the imidazolium ring and fluorine (F) of the $[BF_4]^-$ anion respectively. However, in the third trial output, oxygen of the first $SiO_2$ molecule (near the H-C(4)-C(5)-H) interacts with H-C(5) and in second $SiO_2$ molecule, oxygen again interacts with C(2)-H and Si of $SiO_2$ is interacted with F of the $[BF_4]^-$ anion as observed in trial run 2. Overall, these theoretical calculations confirm the interactions of IL molecules with the pore wall surface of MCM-41 as we have observed in the experimental FTIR spectra. Both the experimental and

theoretical results confirm that C-H vibrations of imidazolium ring and vibrations related to anion $[BF_4]^-$ are more affected.

### 3.8. Fluorescence

The fluorescence emission spectra of bulk IL ([EMIM][$BF_4$]) and typical fluorescence emission spectra of sample MW-5 (containing higher amount of IL after surface adsorbed washed IL) are shown in Fig. 13a and 13b. bulk IL (Fig. 13a) is found to fluoresce with the excitation wavelength ($\lambda_{ex}$) from 280 to 330 nm. The emission band ($\lambda_{em}$) exhibited a remarkable shift from 510 to 490 nm with $\lambda_{ex}$ from 280 to 330 nm i.e. fluorescence emission of bulk [EMIM][$BF_4$] was strongly dependent on the excitation wavelength. However, after being confined typical fluorescence emission spectra of sample MW-5 (Fig. 13b) shows the fluorescence emission peak at 369 nm with the excitation wavelength $\lambda_{ex}$ from 265 to 285 nm. Thus the fluorescence emission of sample MW-5 is independent of the excitation wavelength. The emission observed at these frequencies shows a blue shift (with respect to bulk IL emission). So, IL [EMIM][$BF_4$] in ordered nano pore space shows fluorescence emission which is blue shifted which may be due to the stacking of IL cation as reported by Zhang et al. for IL [EMIM][$N(CN)_2$].[73]

### Conclusions

In the present work, we have found that during confinement of IL into the pores of MCM-41, some IL [EMIM][$BF_4$] was adsorbed on the external surface of pore walls of MCM-41 nanoparticles and remaining IL confined into the pores. The surface absorbed IL was successfully removed and the properties of IL were studied in confined system only. The glass transition temperature $T_g$ of IL was found to change upon confinement compared to the bulk IL. The glass transition temperature increased compared to the bulk IL. Other phase transition

temperatures; crystallization temperature $T_c$ and melting temperature $T_m$ of IL was not found due to the ordered porous nature of supporting material. It was also found that the thermal stability of IL into ordered porous system decreased and depends upon ionic liquid loading. Moreover, FTIR spectroscopy confirmed the strong interaction of the IL with the silica surface. C-H vibrational frequencies related to the alkyl chain are less affected while the aromatic ring C-H vibrations of the ionic liquid change more on confinement in pores. Due to small surface density of hydroxyl groups in MCM-41, the dominant interaction of IL inside pores is with O-Si-O. The theoretical calculations of interactions suggest that the anion of IL prefers to interact with Si of $SiO_2$, but H-C of cation ring prefers to interact with O of $SiO_2$. This result is also confirmed by FTIR studies in which Si-O band, Si-O-Si and anion band changed more with respect to H-C of the cation ring. Fluorescence spectrum shows that a blue shift after incorporation of IL in MCM-41 pores.

**Acknowledgements**

One of us (R.K.S.) is thankful to DST, New Delhi and BRNS-DAE, India for providing financial assistance. A.K.T. and Y.L.V. are thankful to CSIR, New Delhi, India for award of Junior Research Fellowship (JRF) and Senior Research Fellowship (SRF) respectively. We are also thankful to Prof. Il-Kwon Oh, KAIST, Korea for providing SEM and TEM images of our samples.

## References


1. P. Wasserscheid and T. Welton, *Ionic Liquids in Synthesis;* Wiley-VCH Verlag: Weinheim, 2003.
2. M. Armand, F. Endres, D. R. MacFarlane, H. Ohno and B. Scrosati, *Nat. Mater*., 2009, **8**, 621.
3. J. L. Anderson, J. Ding, T. Welton and D.W. Armstrong, *J. Am. Chem. Soc*., 2002, **124**, 14247.
4. T. Welton, *Chem. Rev.*, 1999, **99**, 2071.
5. D. Wei and A. Ivaska, *Anal. Chim. Acta.*, 2008, **607**,126.
6. J. K. Chang, W. T. Tsai, P. Y. Chen, C. H. Huang, F. H. Yeh and I. W. Sun, *Electrochem. Solid St.,* 2007, **10**, A9.
7. S. Seki, Y. Mita, H. Tokuda, Y. Ohno, Y. Kobayashi, A. Usami, M. Watanabe, N. Terada and H. Miyashiro, *Electrochem. Solid St.,* 2007, **10**, A237.
8. A. Berthod, M. J. Ruiz-Angel and S. Carda-Broch, *J. Chromatogr. A,* 2008*,* **1184**, 6.
9. R. D. Rogers and K. R. Seddon, *Ionic Liquids: Industrial Applications to Green Chemistry;* ACS Symposium Series American Chemical Society, Washington, 2002.
10. J. L. Bideau, L. Viau and A. Vioux, *Chem. Soc. Rev.,* 2011, **40**, 907.
11. A. I. Horowitz and M. J. Panzer, *J. Mater. Chem*., 2012, **22**, 16534.
12. M. Bracheta, T. Broussea and J. Le. Bideaua, *ECS Electrochem. Lett.,* 2009, **3**, A112.

13. R. F. de Souza, J. C. Padilha, R. S. Gonc, Alves and J. Dupont, *Electrochem. Commun.,* 2003, **5**, 728.

14. P. Wang, S. M. Zakeeruddin, J. E. Moser and M. Gratzel, *J. Phys. Chem. B,* 2003, **107**, 13280.

15. D. R. Macfarlane, M. Forsyth, P. C. Howlett, J. M. Pringle, J. Sun, G. Annat. W. Neil and E.I. Izgorodina, *Accounts. Chem. Res.,* 2007, **40**, 1165.

16. Y. Liu, M. Wang, J. Li, Z. Li, P. He, H. Liu and J. Li, *Chem. Commun*., 2005, **13**, 1778.

17. M. P. Singh, R. K. Singh and S. Chandra, *J. Phys. Chem. B,* 2011, **115**, 7505.

18. M. P. Singh, R. K. Singh and S. Chandra, *J. Phys. D: Appl. Phys.,* 2010, **43**, 092001.

19. M. Sha, G. Wu, Y. Liu, Z. Tang and H. Fang, *J. Phys. Chem. C,* 2009, **113**, 4618.

20. M. A. Neouze, J. L. Bideau, P. Gaveau, S. Bellayer and A. Vioux, *Chem. Mater*., 2006, **18**, 3931.

21. A. K. Gupta, M. P. Singh, R. K. Singh and S. Chandra, *Dalton T.,* 2012, **41**, 6362.

22. L. Viau, M. A. Neouze, C. Biolley, S. Wolland, D. Brevet, P. Gaveau, P. Diudonne, A. Galarneau and A. Vioux, *Chem. Mater*., 2012, **24**, 3128.

23. Y. Xia, R. Mokaya, G. S. Walker and Y. Zhu, *Adv. Energy Mater.,* 2011, **4**, 678.

24. K. L. Stefanopoulos, G. E. Romanos, O. C. Vangeli, K. Mergia, N. K. Kanellopoulos, A. Koutsioubas and D. Lairez, *Langmuir,* 2011, **27**, 7980.

25. L. L. Lou, X. Peng, K. Yu and S. Liu, *Catal. Commun.,* 2008, **9**, 1891.

26. C. Yuan, Z. Huang and J. Chen, *Catal. Commun.,* 2012, **24**, 56.

27. P. M. Page, T. A. McCarty, G. A. Baker, S. N. Baker and F. V. Bright, *Langmuir,* 2007, **23***,* 843.

28. P. Van Der Voort, D. Esquivel, E. De Canck, F. Goethals, I. Van Driessche and F. J. Romero-Salguero*, Chem. Soc. Rev.,* 2013, **42**, 3913.

29. V. Guillerm, D. Kim, J. F. Eubank, R. Luebke, X. Liu, K. Adil, M. S. Lah and M. Eddaoudi, *Chem. Soc. Rev,* 2014, **43**, 6141.

30. X. Feng, X. Ding and D. Jiang, *Chem. Soc. Rev.,* 2012*,* **41**, 6010.

31. M. Vallet-Regi, F. Balas and D. Arcos, *Angew. Chem. Int. Ed.,* 2007, **46**, 7548.

32. L. Frunza, S. Frunza, A. Schonhals, U. Bentrup, R. Fricke, I. Pitsch and H. Kosslick, *Stud. Surf. Sci. Catal.,* 2002, **142**, 1323-1330.

33. Z. Zhou and M. Hartmann, *Chem. Soc. Rev.,* 2013, **42**, 3894.

34. A. Taguchi and F. Schuth, *Micropor. Mesopor. Mat.,* 2005, **77**, 1.

35. T. Selvam, A. Machoke and W. Schwieger, *Appl. Catal. A-Gen.,* 2012, **445–446**, 92.

36. O. C. Vangeli, G. E. Romanos, K. G. Beltsios, D. Fokas, E. P. Kouvelos, K. L. Stefanopoulos and N. K. Kanellopoulos, *J. Phys. Chem. B,* 2010, **114**, 6480

37. S. Liang, Y. Zhou, H. Liu, T. Jiang and B. Han, *Catal. Lett*., 2010, **140**, 49.

38. X. Ma, Y. Zhou, J. Zhang, A. Zhu, T. Jiang and B. Han, *Green Chem*., 2008, **10**, 59.

39. B. Gadenne, P. Hesemann, and J. J. Moreau, *Chem. Commun*, 2004, **15**, 1768.

40. M. H. Valkenberg and W. F. Hölderich, *Green Chemistry*, 2002, **4**, 88.

41. M. P. Singh, R. K. Singh and S. Chandra, *Prog. Mater. Sci.,* 2014, **64**, 73.

42. A. Manna and A. Kumar, *Chem. Phys. Chem.*, 2014, **15**, 3067.

43. S. Tiwari and A. Kumar, *Angewandte Chemie Int. Ed.*, 2006, **45**, 4824.

44. G. Singh and A. Kumar, *Indian J. Chem.*, 2008, **47A**, 495.

45. R. Mu and M. Malhotra, *Phys. Rev. B*: *Condens. Matter,* 1991, **44**, 4296.

46. K. Morishige and K. Kawano, *J. Chem. Phys*., 1999, **110**, 4867.

47. A. Serghei, M. Tress, J. R. Sangoro and F. Kremer, *Phys. Rev. B,* 2009, **80**, 184301.

48. P. B. Macedo, C. T. Moynihan and R. Bose, *Phys. Chem. Glasses,* 1972, **13**, 171.

49. S. J. Gregg and K. S. W. Sing, *Adsorption, Surface Area and Porosity*, 2nd ed: Academic Press: New York, 1991**.**

50. K. S. W. Sing, D. H. Everett, R. A. W Haul, L. Moscou, R. A. Pierotti, J. Rouquerol and T. Siemieniewska, *Pure Appl. Chem.,* 1985*,* **57**, 603.

51. S. Brunauer, P. H. Emmett and E. Teller, *J. Am. Chem. Soc.,* 1938, **60**, 309.

52. Y. L. Verma, M. P. Singh and R. K. Singh, *J. Nanomater.,* 2012, **2012**.

53. S. Hudson, D. A. Tanner, W. Redington, E. Magner, K. Hodnett and S. Nakahara, *Phys. Chem. Chem. Phys.,* 2006, **8**, 3467.

54. X. S. Zhao, G. Q. Lu, A. K. Whittaker, G. J. Millar and H. Y. Zhu, *J. Phys. Chem. B,* 1997, **101**, 6525.

55. A. K. Gupta, Y. L. Verma, R. K. Singh and S. Chandra, *J. Phys. Chem. C,* 2014**, 118**, 1530.

56. F. Fajula and D. Brunel, *Micropor. Mesopor. Mat.,* 2001, **48**, 119.

57. C. J. Brinker and G.W. Scherer, *Sol-Gel Science;* Academic Press: Boston San Diego New York, 1990.

58. S. A. M. Noor, P. M. Bayley, M. Forsyth and D. R. MacFarlane, *Electrochim. Acta*., 2013, **91**, 219.

59. S. A. Katsyuba, E. E. Zvereva, A. Vidis and Paul J. Dyson, *J. Phys. Chem. A* 2007, **111**, 352.

60. F. Shi and Y. Deng, *Spectrochim. Acta*., 2005, **62**, 239.

61. P. A. Hunt, B. Kirchner and T. Welton, *Chem. Eur. J.,* 2006, **12**, 6762.

62. S. Kossmann, J. Thar, B. Kirchner, P.A. Hunt and T. Welton, *J. Chem. Phys*., 2006, **124**, 174506.

63. S. Zahn, G. Bruns, J. Thar and B. Kirchner, *Phys. Chem. Chem. Phys*., 2008, **10**, 6921.

64. E. I. Izgorodina and D. R. MacFarlane*, J. Phys. Chem. B,* 2011, **115**, 14659.

65. D. R. MacFarlane, J. M. Pringle, K. M. Johansson, S. A. Forsyth and Maria Forsyth, Chem. Commun., 2006, **18**, 1905.

66. N. E. Heimer, R. E. Del Sesto, Z. Meng, J. S. Wilkes and W. R. Carper, *J. Mol. Liq.*, 2006, **124**, 84.

67. S. A. Katsyuba, P. J. Dyson, E. E. Vandyukova, A. V. Chernova and A. Vidis, *Helvetica Chimica Acta*, 2004, **87**, 2556.

68. M. A. Alibeik and M. Pouriayevali, *Catal. Commun*., 2012, **22**, 13.

69. M. J. Frisch, G. W. Trucks, H. B. Schlegel, G. E. Scuseria, M. A. Robb, J. R. Cheeseman, G. Scalmani, V. Barone, B. Mennucci, G. A. Petersson, H. Nakatsuji, M. Caricato, X. Li, H. P. Hratchian, A. F. Izmaylov, J. Bloino, G. Zheng, J. L. Sonnenberg, M. Hada, M. Ehara, K. Toyota, R. Fukuda, J. Hasegawa, M. Ishida, T. Nakajima, Y. Honda, O. Kitao, H. Nakai, T. Vreven, J. A. Montgomery, Jr., J. E. Peralta, F. Ogliaro, M. Bearpark, J. J. Heyd, E. Brothers, K. N. Kudin, V. N. Staroverov, R. Kobayashi, J. Normand, K. Raghavachari, A. Rendell, J. C. Burant, S. S. Iyengar, J. Tomasi, M. Cossi, N. Rega, N. J. Millam, M. Klene, J. E. Knox, J. B. Cross, V. Bakken, C. Adamo, J. Jaramillo, R.

Gomperts, R. E. Stratmann, O. Ya zyev, A. J. Austin, R. Cammi, C. Pomelli, J. W. Ochterski, R. L. Martin, K. Morokuma, V. G. Zakrzewski, G. A. Voth, P. Salvador, J. J. Dannenberg, S. Dapprich, A. D. Daniels, O. Farkas, J. B. Foresman, J. V. Ortiz, J. Cioslowski and D. J. Fox, *Gaussian 09, Revision A.02, Gaussian, Inc., Wallingford CT,* 2009.

70. A. D. Becke, *J. Chem. Phys.,* 1993, **98**, 5648.
71. C. Lee, W. Yang and R. G Parr, *Phys. Rev. B,* 1988, **37**, 785.
72. R. Dennington, T. Keith and J. Millam, *Gauss View,* 2009, ***Version 5.***
73. J. Zhang, Q. Zhang, F. Shi, S. Zhang, B. Qiao, L. Liu, Y. Ma and Y. Deng, *Chem. Phys. Lett*., 2008, **461**, 229.

**Table 1**. Pore parameters of different samples as determined by BET analysis.

| | BJH Desorption Volume ($cm^3/g$) | BET Surface Area ($m^2/g$) | Porosity $\phi$ (%) | BET Constant C |
|---|---|---|---|---|
| Pristine MCM-41 | 0.84 | 764 | 65 | 96 |
| MW-3 | 0.24 | 36 | 35 | 81 |
| MW-4 | 0.18 | 45 | 29 | 49 |
| MW-5 | 0.17 | 59 | 27 | 35 |

**Table 2**. Onset temperature of bulk IL and confined IL in various amount in MCM-41.

| Sample | Onset | Decomposed Mass% |
|---|---|---|
| bulk IL | 437 | 98 |
| MW-3 | 369 | 20 |
| MW-4 | 374 | 28 |
| MW-5 | 389 | 33 |

**Table 3.** Vibrational bands and their assignments[25,26,58,59,66-68] of bulk IL, MW-3, MW-4, MW-5 and pristine MCM-41.

| Assignment | Bulk IL | MW-3 | MW-4 | MW-5 | Pristine MCM-41 |
|---|---|---|---|---|---|
| υ(H–C(4)), υ(H–C(5)) stretching of the ring | 3167 | 3163 | 3164 | 3163 | ---- |
| υ(H–C(2)) stretching of the ring | 3123 | 3119 | 3118 | 3117 | ---- |
| aliphatic C-H vibration of the ring | 2993, 2950, 2890 | ---- | 2996 | 2995 | ---- |
| $BF_4$ asymmetric stretching | 1173 | 1169 | 1168 | 1168 | ---- |
| $BF_4$ asymmetric stretching | 1116 | 1124 | 1122 | 1118 | ---- |
| Internal asymmetric Si-O | ---- | 1084 | 1084 | ---- | 1086 |
| $BF_4$ asymmetric stretching, $(N)CH_2$ and $(N)CH_3$ CN stretching | 1060 | 1063 | 1064 | ---- | ---- |
| $BF_4$ asymmetric stretching | 1024 | 1034 | 1036 | 1047 | ---- |
| Symmetric stretching of Si-OH | ---- | 980 | 978 | 976 | 969 |
| Stretching of Si-O | ---- | 791 | 796 | 795 | 800 |
| $BF_4$ stretching | 757 | 741 | 743 | 746 | ---- |
| Bending of Si-O-Si | ---- | 461 | 460 | 458 | 464 |

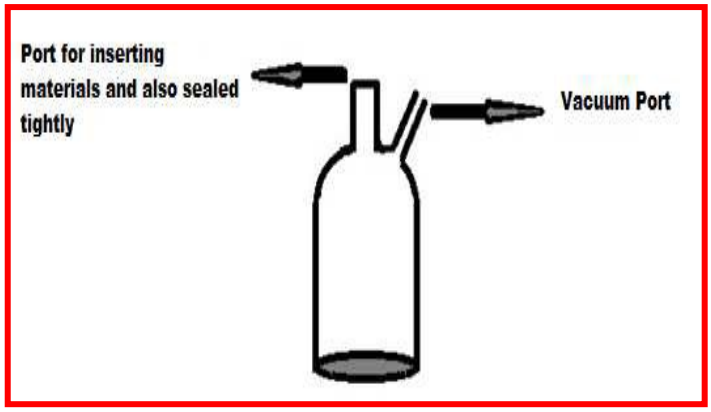


**Fig. 1** Schematic representation of used vial in which synthesis procedure was completed.

**Fig. 2** Typical photograph of ionic liquid confined MCM-41.

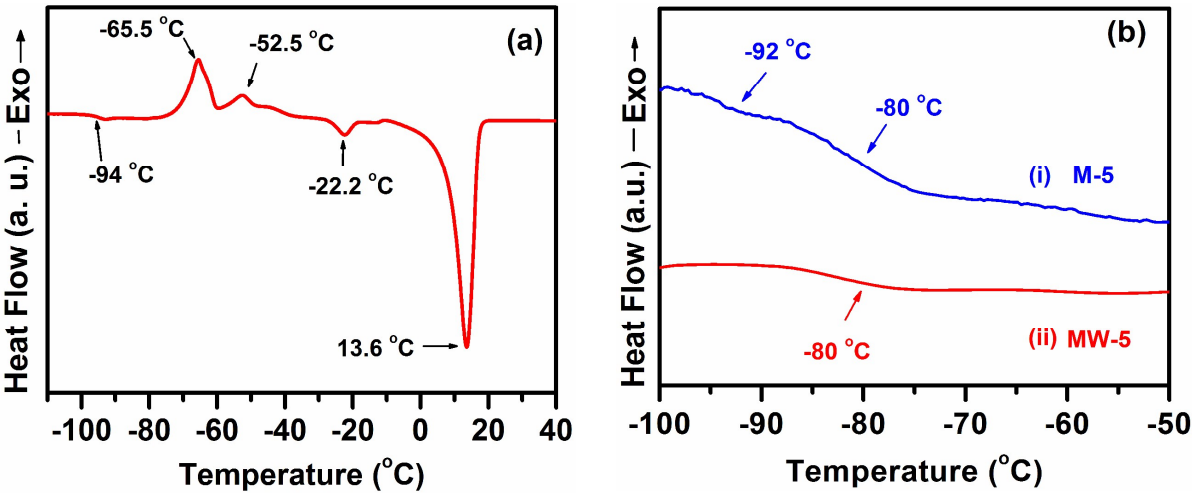


**Fig. 3** Differential scanning calorimetry (DSC) heating curves for (a) bulk IL [EMIM][$BF_4$] and (b) (i) M-5 and (ii) MW-5.

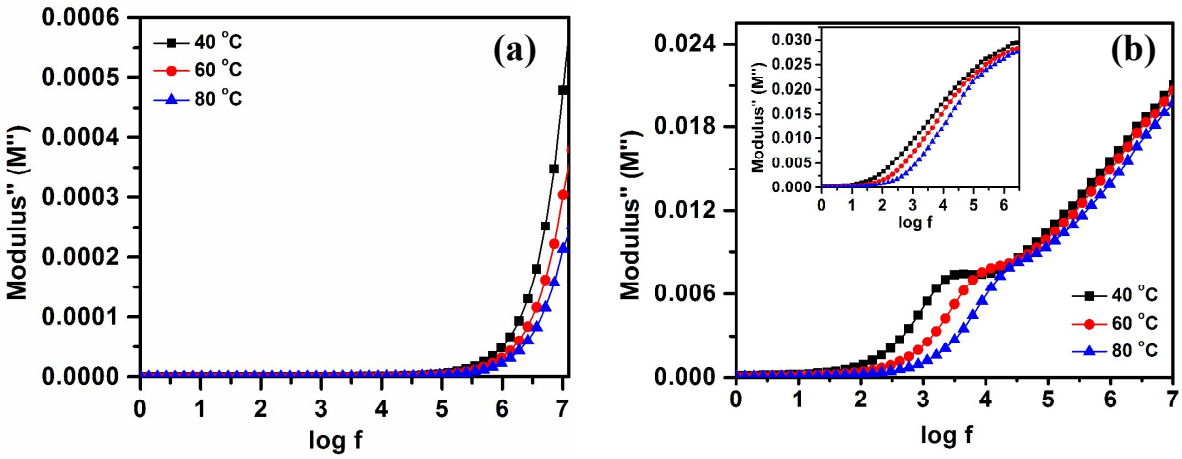


**Fig. 4** Modulus vs frequency (M'' vs log f) for (a) bulk IL [EMIM][$BF_4$]; (b) M-3 and MW-3 (inset).

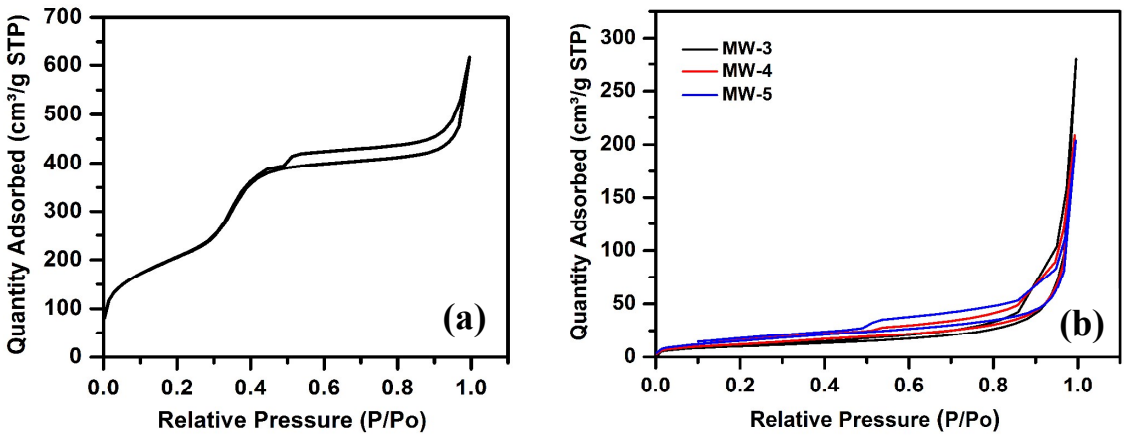


**Fig. 5** $N_2$-sorption isotherms of (a) pristine MCM-41 and (b) washed sample obtained with different IL loading.

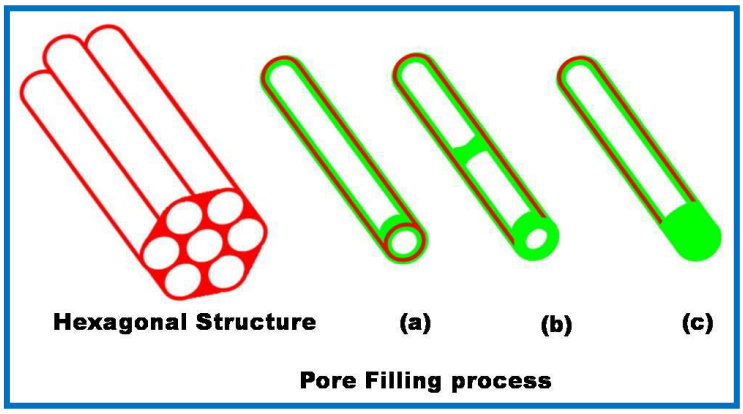


**Fig. 6** Various types of filling process (a) primary pore filling (b) increasing amount into pores (c) surface adsorption on pore mouth.

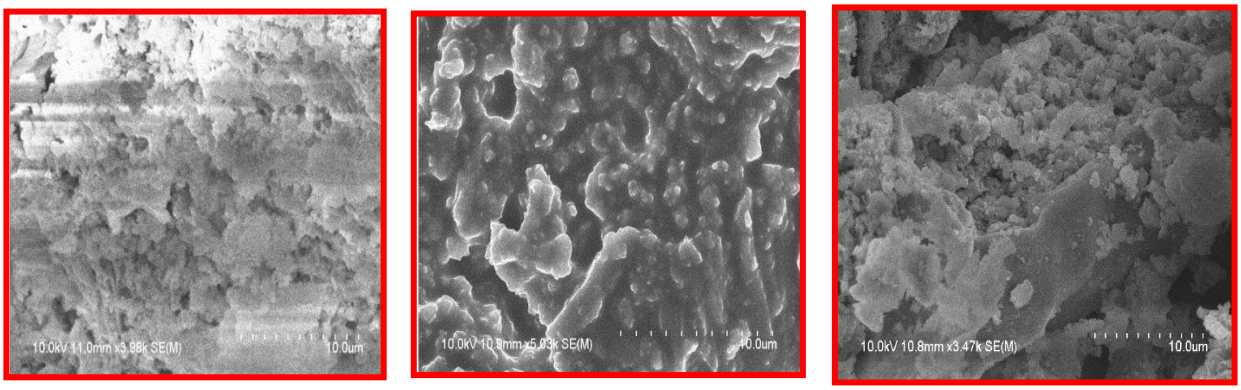


**(a)** **(b)** **(c)**

**Fig. 7** SEM images of (a) pristine MCM-41 (b) without surface wash sample M-5 and (c) after surface wash sample MW-5.

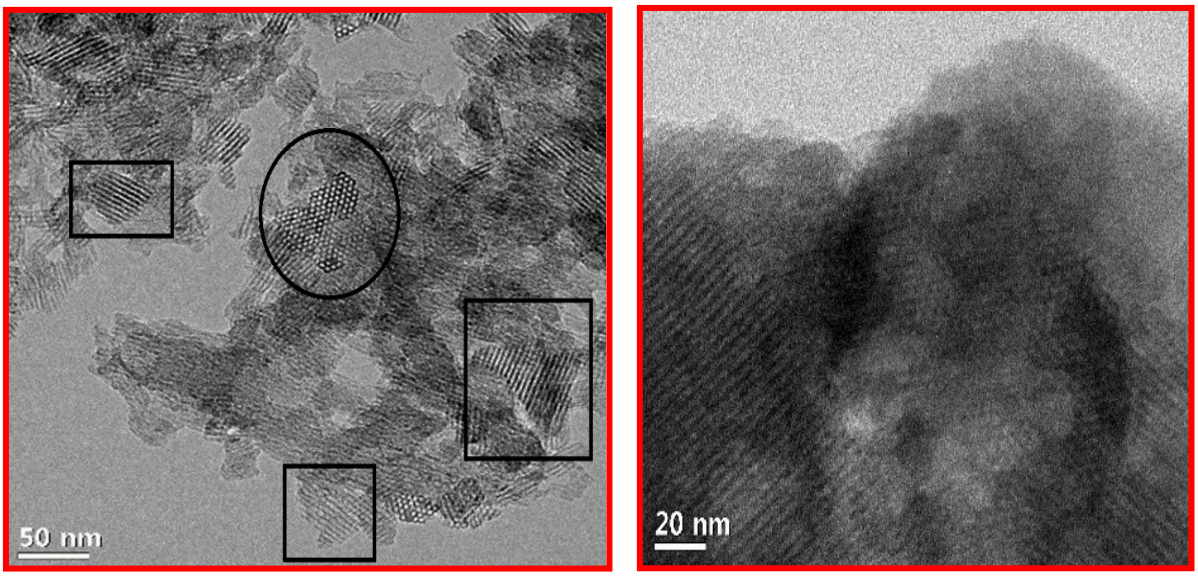


**Fig. 8** TEM images of (a) pristine MCM-41 and (b) MCM-41 with confined IL (MW-5).

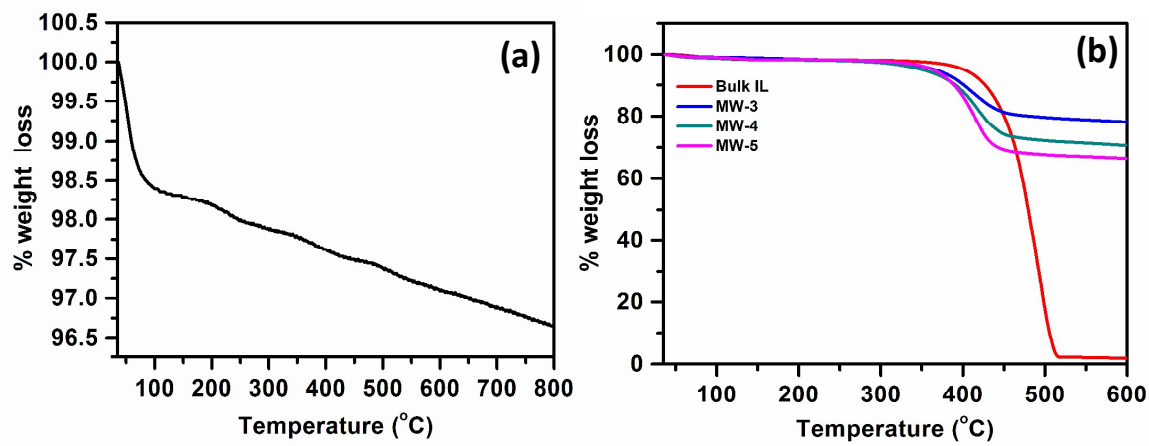


**Fig. 9** TGA thermograms of (a) pristine MCM-41 and (b) bulk and confined IL [EMIM][$BF_4$].

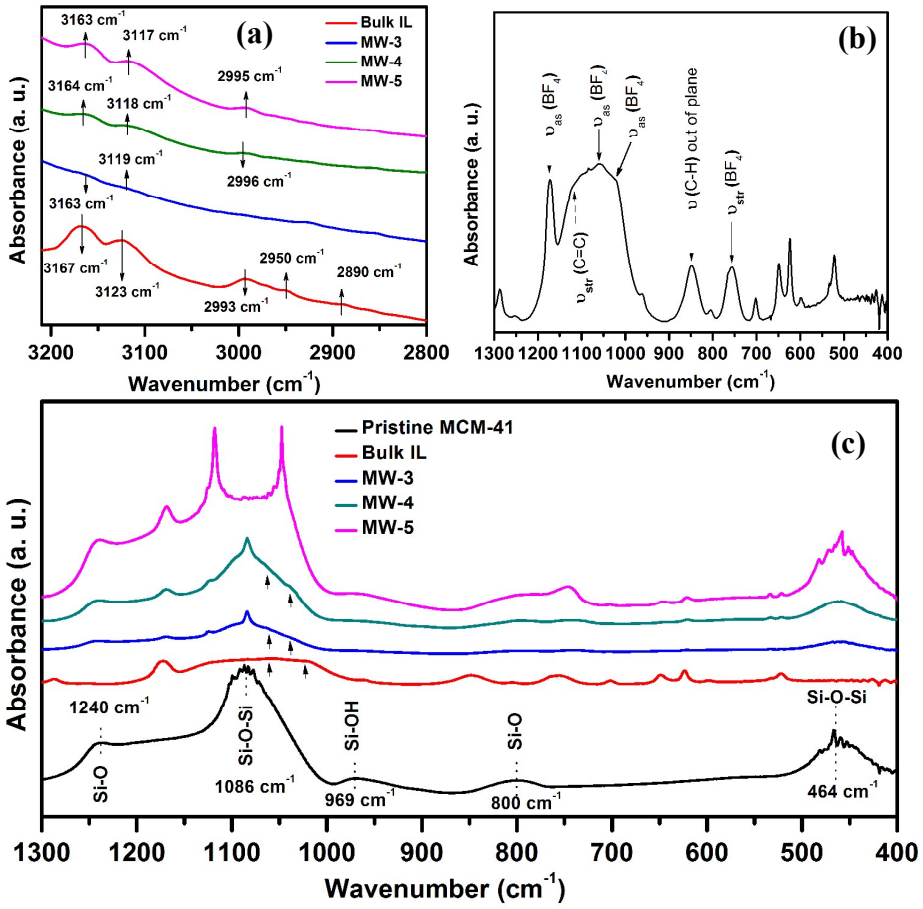


**Fig. 10** (a) FTIR spectra of bulk IL and samples (MW-3, MW-4 and MW-5) in the range 3210-2800 $cm^{-1}$; (b) FTIR spectra of bulk IL in spectral range 1300-400 $cm^{-1}$ (c) FTIR spectra of pristine MCM-41, bulk IL and samples in the range of 1300-400 $cm^{-1}$.

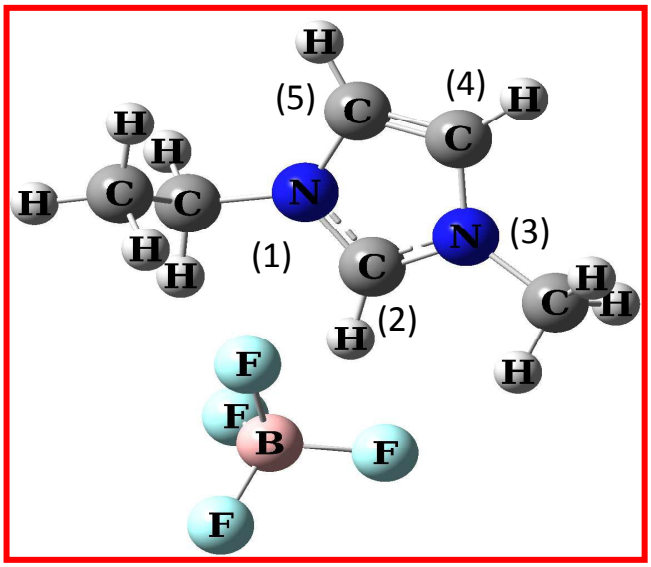


**Fig. 11** Optimized geometry of IL cation and anion.

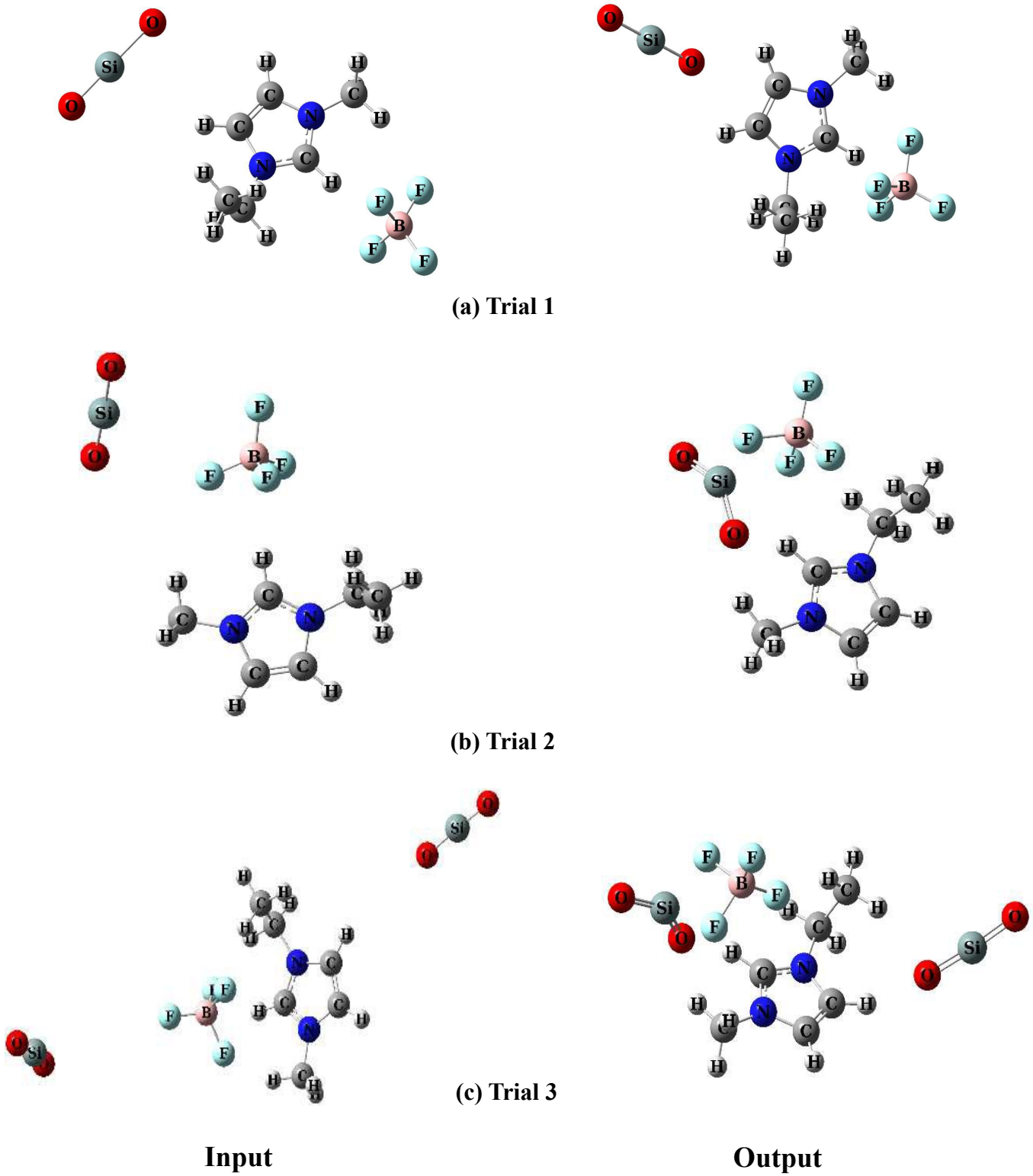


**Fig. 12** Different trial inputs and corresponding outputs for optimized interaction for IL [EMIM][$BF_4$], showing (a) interaction of IL-cation ring hydrogen with O present on the surface of silica pore-wall or MCM-41 matrix, (b) IL-anion with Si of matrix and (c) cation and anion interact individually with $SiO_2$ matrix: where (●) silicon, (●) oxygen, (●) nitrogen, ( ) hydrogen, ( ) carbon, (●) boron, (●) fluorine atom.

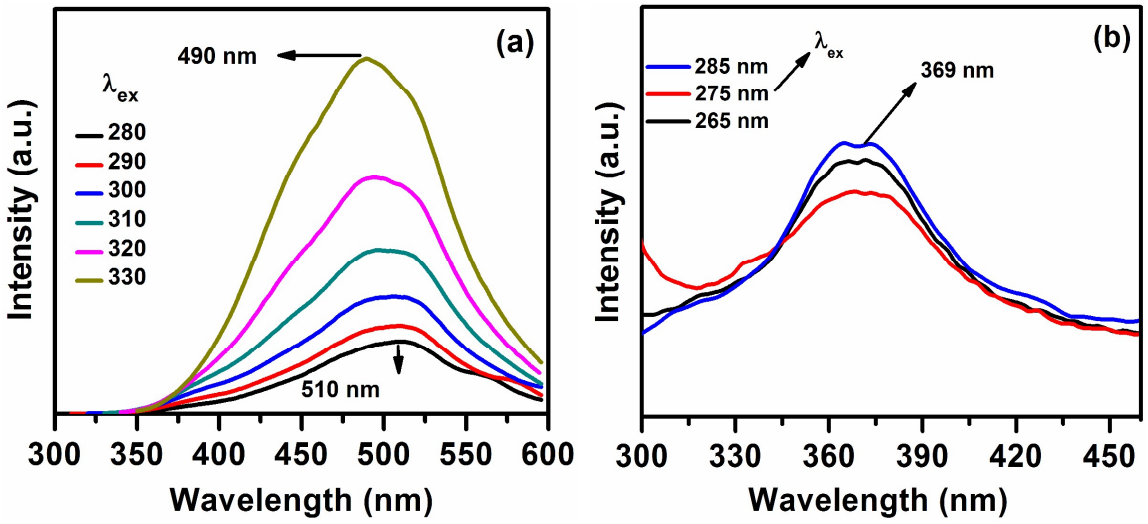


**Fig. 13** Fluorescence spectra of (a) bulk IL and (b) MW-5.

# Graphical Abstract